SELECTED TOPICS ON STIMULATED RAMAN EFFECT

FINAL REPORT

for the period

1 October 1966 - 30 September 1968

ONR Contract No N0014-67-A-0112-0015
ARPA Order Number 306
NR 015-822/10-17-66
Principal Investigator: R. H. Pantell

M. L. Report No. 1730

March 1969

Microwave Laboratory
W. W. Hansen Laboratories of Physics
Stanford University
Stanford, California

TABLE OF CONTENTS

BLANK PAGE

I. TUNABLE INFRARED GENERATION BY RAMAN SCATTERING

(R. H. Pantell, B. C. Johnson, Jr. and S. S. Sussman)

A. INTRODUCTION

Nonlinear characteristics in various materials may under certain conditions give rise, either spontaneously or in a stimulated manner, to the mixing of source frequencies and resonant frequencies indigenous to the material. This mixing then serves to produce sum and difference frequencies. The special case where the material resonant frequency is an optical vibrational mode is called the Raman effect. Raman scattering generally involves a source frequency, typically in the visible (0.4-0.7 μ) region of the spectrum, interacting with an optical mode in the infrared or far infrared (1-1000 μ). It is this infrared frequency which in turn represents the difference between source and Stokes (or anti-Stokes) frequencies. Spontaneous Raman scattering and the generation of Stokes light has been extensively studied, both in theory and experiment.[1] However, Raman scattering from the infrared active transition also produces electromagnetic radiation at the vibrational frequency. The purpose of this project has been to undertake a study of this infrared radiation produced by the spontaneous Raman effect.

---

[1] H. E. Puthoff, R. H. Pantell, G. B. Huth, and M. A. Chacon, "Near-Forward Raman Scattering in $LiNbO_3$," J. Appl. Phys. 39, 4 (March 1968). See also, H. E. Puthoff, "The Stimulated Raman Effect and Its Application as a Tunable Laser." Microwave Laboratory Report No. 1547, Stanford University. A complete history of the Raman effect literature is contained in the bibliography.

The theoretical analysis outlined below has predicted the existence of tunable infrared radiation output detectable in the far infrared. For the case of the 628 cm^{-1} mode of $LiNbO_3$, the far infrared light wavelength tunes continuously from 16-20 μ as the scattering angle is varied. Preliminary estimates indicated that for a pump power of ~ 1 watt (cw), the power level of the total output should be ~ 10^{-9} watts. Forthcoming experimental results are expected to confirm and further document the detailed behavior of the effect.

The results of this study have a number of useful and interesting aspects. The output constitutes a direct measurement of material properties, providing in effect a direct "readout" of the dispersion curve for the particular medium employed. Further understanding of such material properties is a result which may suggest further experiments and possible new uses for nonlinear materials. In particular, the optimization of the effect under study is expected to open the possibility for investigation of the properties of other infrared and Raman active modes (for example: the 248 cm^{-1} mode of $LiNbO_3$).

By utilizing other vibrational modes, as well as the introduction of other nonlinear materials, it would become possible to create tunable infrared sources which cover virtually the entire infrared spectrum. Exploitation of this effect could introduce criteria for new nonlinear materials not presently available for study.

The present source will be tunable over quite a sizeable (16-20 μ) percentage range (for 628 cm^{-1} mode). The other principal mode (248 cm^{-1}) has a tuning range which is potentially even larger, as compared with typical optical tuning ranges (generally on the order of a few percent).

Although the spontaneous effect does not result in large power outputs, the principle of frequency tuning in the infrared remains valid also for the stimulated Raman effect. To date the stimulated Raman effect has not been observed in $LiNbO_3$; however, its potential existence in this or other nonlinear materials would make available kilowatts (or possibly more) of pulsed power, tunable in the infrared. Such highly monochromatic tunable sources are not presently available at infrared frequencies and would prove highly desirable and versatile for applications in such areas as communications, detection and warning systems, information storage and readout, tracking and other astronautical applications, in addition to many scientific areas such as spectroscopy, solid state physics, and the study of material properties.

B. EXPERIMENT

In order to satisfy the experimental requirement for a relatively high power laser source with an output of 1-2 watts total cw power, it was decided to construct an rf excited argon-ion gas laser. By virtue of constructing the laser it became possible to incorporate many features into the design which make the system unusually flexible and reliable, and also has resulted in a working system at considerably less expense than comparable commercially available argon lasers.

The laser system (see Fig. 1) was completed in September 1967. Efforts since that time have been concentrated largely in optimizing the laser's performance and reliability. The system is presently operating with a total output power of ~ 1.25 watts in all the lines and somewhat over 500 MW in the 4880 Å line. These figures are restricted primarily

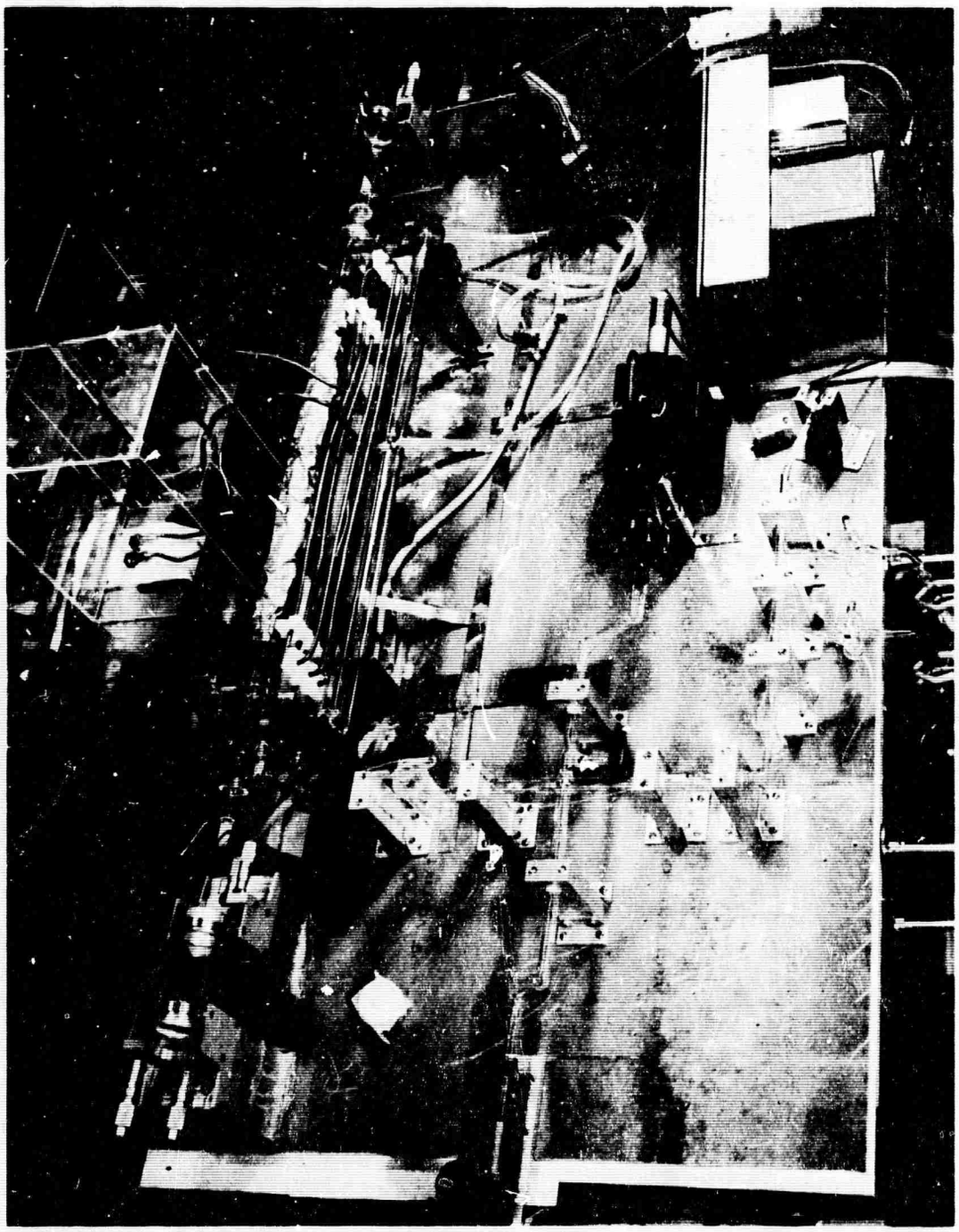

FIG. 1--The Argon-ion laser system

by the fact that they represent the power limit of the present 3 MHz rf power supply.

The laser incorporates several desirable features, among which are:

(1) A self-contained vacuum system, including both low (100 - 10^{-3} torr) and high (Vac-Ion: 10^{-3} - 10^{-7} torr) vacuum pumps. This system allows for adjustement and monitoring of operating gas pressure as well as regular "flushing" of the system.

(2) Isolated supplies of argon gas. Also would allow operation of the system with other laser active gases, e.g., krypton.

(3) Ball-socket construction of end windows allows for relatively easy cleaning and/or replacement of Brewster angle windows.

(4) Interchanging parts. An exact duplicate of the quartz laser tube is available and should the present tube experience a malfunction, it could be easily replaced in a matter of hours.

(5) Mirror flexibility. The external mirror mounts have provided for simplicity of alignment and adjustments of the optical cavity configuration as well as easy interchangeability. The system presently operates with a 6 m spherical (94% reflecting) and a 99% reflecting dielectric coated prism forming the optical cavity, thus allowing laser action at a single frequency only.

This system meets the requirements as a pump source for the present experiment and is sufficiently flexible to be adapted to future experimental demands calling for a cw laser source.

In addition to construction and optimization of the argon-ion laser source, preparations for experimental observation of the spontaneous Raman scattering are virtually completed and preliminary experimental

observations have been initiated. The experimental setup is shown in sketch form in Fig. 2. The laser output is supplied at a single frequency (either 4880 Å or 5145 Å) through a 1 kc chopper which also supplies the reference signal for the Princeton Applied Research phase sensitive detection system. The laser light, acting as an extraordinary wave ($E\|$ to C-axis) enters the uniaxial crystal ($LiNbO_3$) after being focused by the lens to a point at or near the 45° face of the crystal which is specially cut and polished for optimum tuning of the output radiation. At this point, the laser light is totally reflected from the 45° face and effectively leaves the system. The infrared output generated within several microns of the surface exits at various angles to the surface normal. Radiation from a specified solid angle may then be selected, passed through a Jarrel-Ash double monochromator, and finally focused on the Ge:Cu infrared detector which monitors the power output through a Princeton Applied Research phase sensitive detection system and strip chart recorder.

C. THEORY

As indicated above, the infrared radiation under study in the present experiment is tunable with angle depending upon particular material properties and source frequencies involved. A theoretical investigation of the spontaneous Raman scattering phenomenon has been carried out in detail for the case of $LiNbO_3$.

In the Raman process, photons are present at sum and difference frequencies $(\nu_L \pm \nu_{IR})$ as well as ν_{IR} . It is the intention of

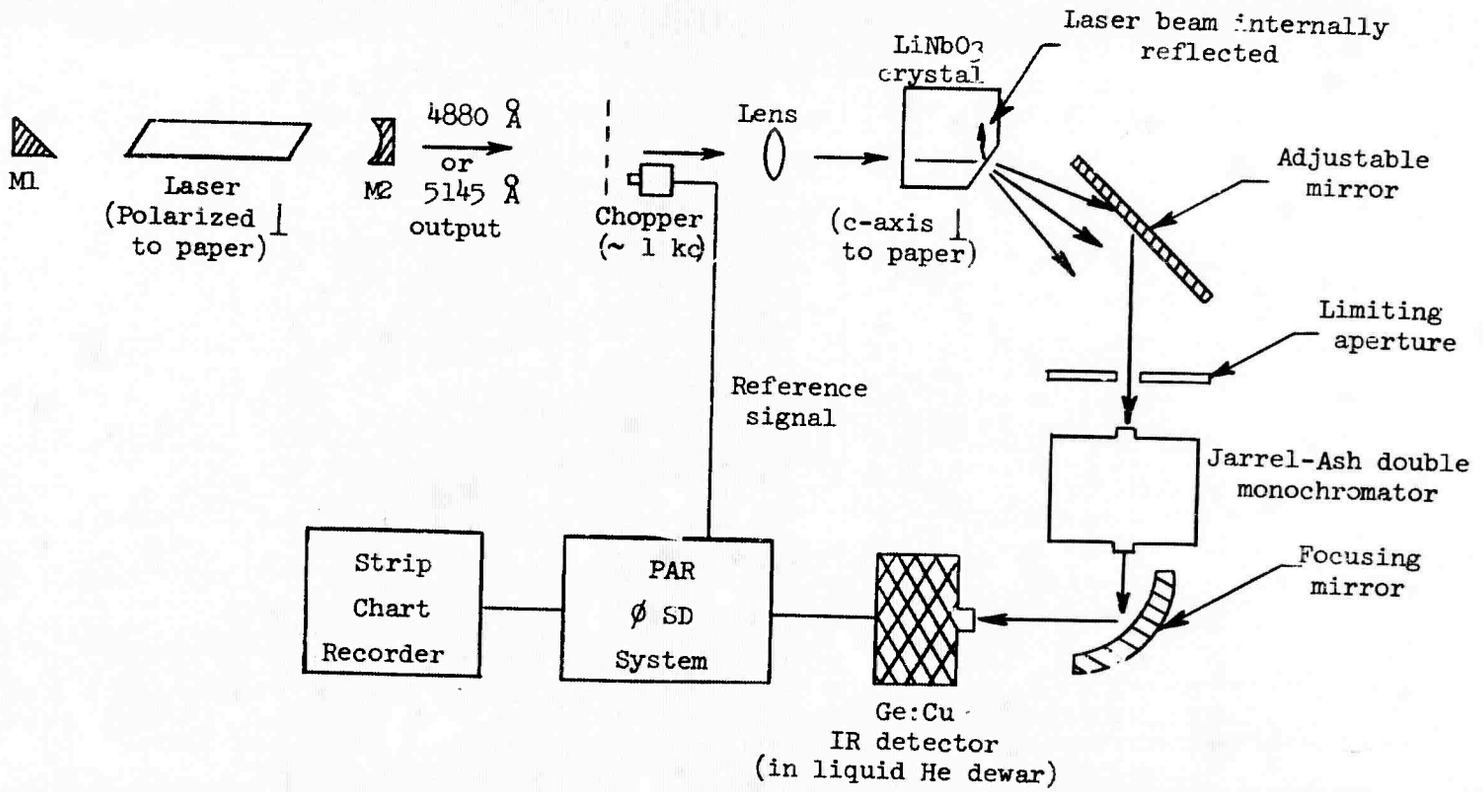

FIG. 2--Experimental arrangement for detection of infrared radiation generated via the spontaneous Raman effect.

the present experiment to investigate and observe directly the output of radiation at the infrared frequency. The experiment will measure the frequency of the output radiation (ν_{IR}) as a function of the angle θ as shown in the diagram (see Fig. 4). Invoking wave vector conservation, we obtain the relation between K_{IR}, the infrared mode wave vector, and the angle θ in the crystal: thus

$$\begin{aligned} K_{IR}^2 &= K_L^2 + K_S^2 - 2K_L K_S \cos\theta \\ &= 4\pi^2(\nu_L n_L - \nu_S n_S)^2 + 8\pi^2 \nu_L \nu_S n_L n_S (1 - \cos\theta) \quad , \end{aligned} \tag{1}$$

where K_L, K_S are the laser and Stokes wave vectors; ν_L, ν_S are the laser and Stokes frequencies in cm^{-1}; and n_L, n_S are the corresponding refractive indices. From the data of Hobden and Warner,[2] we take $n_L = 2.254$, $\nu_L = 20{,}491\ cm^{-1}$, $T = 300^{\circ}K$ and n_S is obtained from the expression

$$n_S = \left\{ 4.5567 + 2.605 \times 10^{-7}\, T^2 + \frac{0.970 \times 10^5 + 2.70 \times 10^{-2}\, T^2}{(10^{14}/\nu_S^2) - (2.01 \times 10^2 + 5.4 \times 10^{-5}\, T^2)} - \frac{2.24 \times 10^6}{\nu_S^2} \right\}^{1/2} . \tag{2}$$

Using the above equations, a computer program was utilized to calculate the data points for the ν_{IR} vs K_{IR} diagram (where $\nu_{IR} = \nu_L - \nu_S$). This calculation yields a family of curves for various angles (θ or α). It is the intersection of these curves with the dispersion characteristic

[2] M. V. Hobden and J. Warner, "The Temperature Dependence of the Refractive Indices of Pure Lithium Niobate," Phys. Letters 22, 3, (15 August 1966).

of the material which ultimately determines the frequency tuning which may be expected in the experiment.

The theoretical dispersion characteristic of $LiNbO_3$ can be constructed from infrared reflectivity data via the expression

$$K_{IR}^2 = \left(\frac{\omega_{IR}}{C}\right)^2 \epsilon = 4\pi^2 \nu_{IR}^2 \epsilon \qquad (3)$$

where K_{IR}, as above, represents the optical mode wave vector and ν_{IR} is the infrared frequency measured in cm^{-1}, and where ϵ, the complex dielectric constant, is given by

$$\epsilon = \epsilon_\infty + \sum_j S_j \nu_j^2 / (\nu_j^2 - \nu_{IR}^2 + i\nu_{IR}\gamma_j) \quad . \qquad (4)$$

In this expression S_j is the strength of the j^{th} transition located at frequency ν_j with bandwidth γ_j and ϵ_∞ is the frequency independent contribution due to high frequency electronic resonances. For the simultaneously Raman and infrared active vibrational modes the dispersion relation becomes partly photon, partly phonon-like. Since $LiNbO_3$ is a negative uniaxial crystal $(n_o > n_e)$ there are two expressions of the above, one for $E\perp$ to C-axis and one for $E\parallel$ to C-axis. For $E\parallel$ to C-axis, it is the A_1 symmetry modes that participate in the interaction and we have taken the data from the oscillator fits of Barker, et al[3]

ν_j (cm^{-1})	S_i	γ_j (cm^{-1})
248	16.0	21
274	1.0	14
307	0.16	25
628	2.55	34
692	0.13	49

$\epsilon_\infty = 4.6$

[3] A.S.Barker, Jr., and R. Loudon, "Dielectric Properties and Optical Phonons in $LiNbO_3$," Phys. Rev. 158, 2 (10 June 1967).

together with the above equation to calculate the theoretical dispersion characteristic. A second computer program was used to calculate solutions to the above relation, resulting in plots of real and imaginary

$$K_{IR} = (4\pi^2 \nu_{IR}^2 \epsilon)^{1/2}$$

as a function of frequency.

Simultaneous plotting of the family of curves (obtained from wave vector conservation) and the dispersion characteristic (real K_{IR} versus ν_{IR}) then results in a series of intersections which determine the extent of possible frequency tuning. The resulting plot is shown below, (Fig. 3) and indicates that as θ varies from 0° to 4° (in crystal) the output frequency varies continuously from ~ 500 - 628 cm^{-1} [~ 16-20 μ] for the 628 cm^{-1} mode, or from ~ 0-248 cm^{-1} [~ 40 $\mu \rightarrow \infty$] for the 248 cm^{-1} mode.

In order to estimate the power and bandwidth available from the spontaneous emission process, we follow a treatment utilized by Puthoff[4] and others.

The resulting equation for the case of spontaneous Raman scattering is given by

$$P_{IR}(\text{watts}) = \left(\frac{\nu_{IR}}{\nu_S}\right)\left(\frac{P_L}{\alpha}\right) \frac{16\pi^2 \hbar \gamma n_S \chi_R''}{3 \epsilon_0^2 n_L \lambda_L \lambda_S^3} \tan^{-1}\left[\frac{\nu - \Omega}{\gamma'/2}\right]\Bigg|_{\nu_1}^{\nu_2}$$

[4] R. H. Pantell and H. E. Puthoff, Notes.

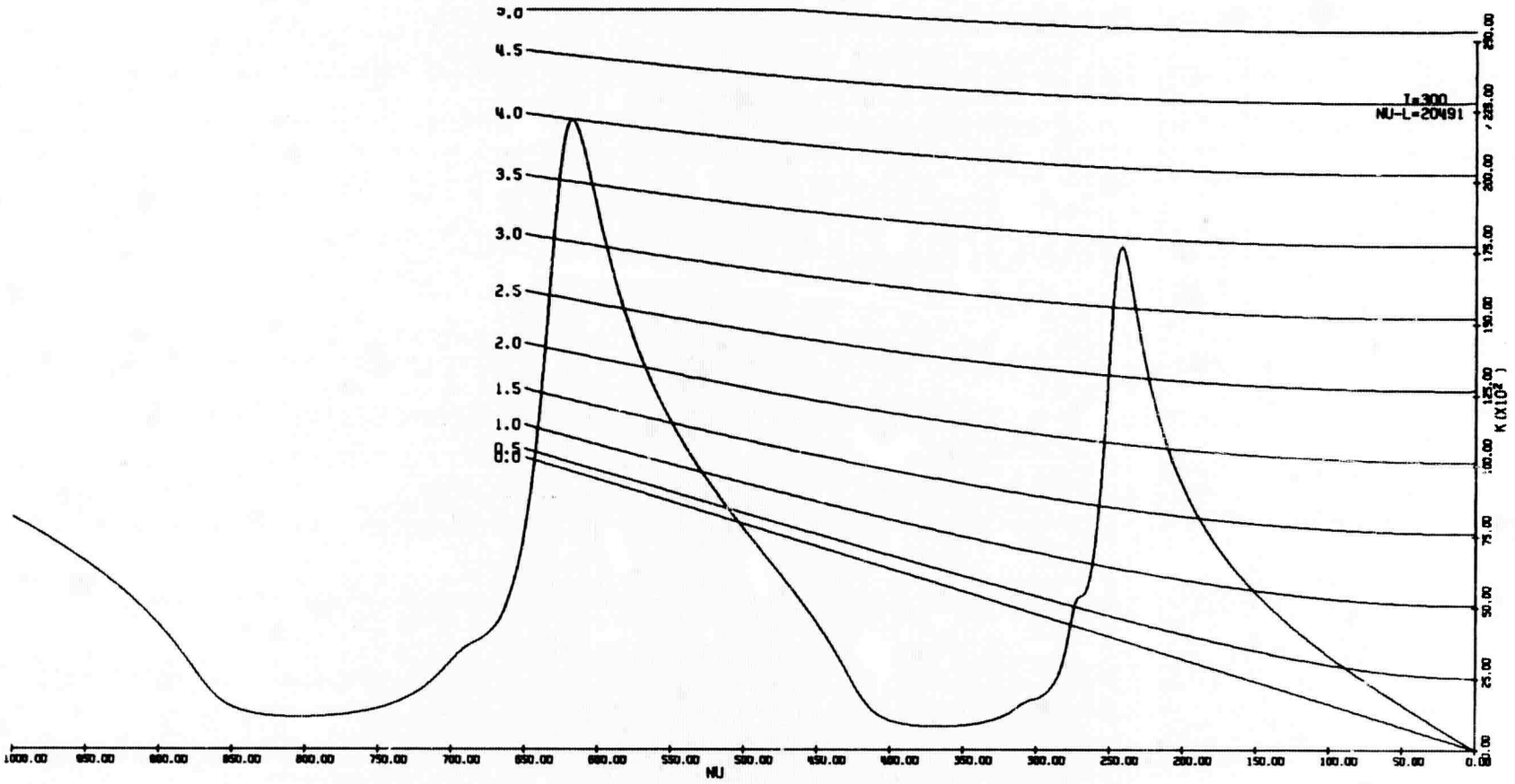

FIG. 3--Computer plot of ν_{IR} vs K_{IR} . The solid curve is the theoretical ir dispersion characteristic based on ir reflectivity measurements. The intersecting family of lines represent frequency-wave vector conservation curves for various angles θ between Stokes and laser beams. The plot is constructed for $LiNbO_3$ at a temperature of 300°K and a laser source wavelength of 4880 Å.

where $\nu_{IR} = \nu_L - \nu_S$, and

P_L = incident laser power (watts)

$\hbar$ = Planck constant/2π (MKS)

γ = linewidth of optical mode (in radians/second)

γ' = linewidth of optical mode (in cm^{-1})

Ω = optical mode center frequency (in cm^{-1})

ϵ_0 = free space permittivity = 8.85×10^{12} f/m

χ_R'' = Raman susceptibility (experimental parameter)

λ_L, λ_S = laser, Stokes wavelengths (in m)

n_L, n_S = laser, Stokes refractive indices

α = infrared absorption coefficient (in m^{-1})

For the $LiNbO_3$, 628 cm^{-1} mode, the relevant parameters are $\chi_R'' = 3 \times 10^{-31}$ MKS, $\Omega = 620$ cm^{-1}, $\gamma' = \gamma/2\pi C = 34$ cm^{-1}; for a 4800 Å pump frequency $\lambda_L = 4.88 \times 10^{-7}$ m , $n_L = 2.25$, $n_S = 2.25$, $\alpha \sim 2 \times 10^5$ m^{-1}.

Inserting the appropriate values into the above relation, we obtain the output power in the infrared mode for a given frequency range, $(\nu_2 - \nu_1)$. The results of this calculation indicate expected power outputs of $\approx 2 \times 10^{-11}$ watts in ≈ 8 - 10 cm^{-1} bandwidths over the tunable region of the infrared output. Such power levels and bandwidths are compatible with the detection ranges of existing experimental equipment.

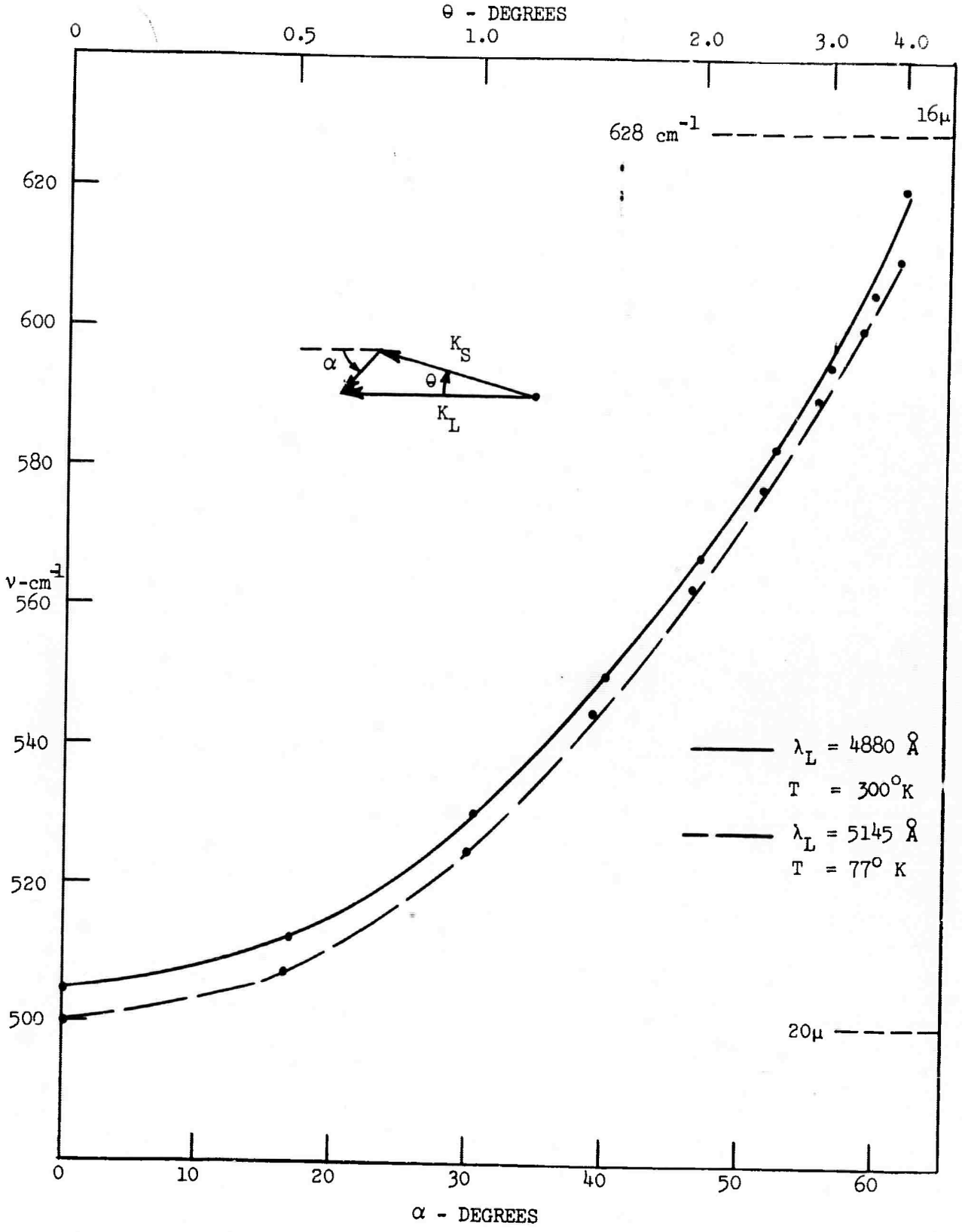

FIG. 4--A plot of infrared frequency output vs scattering angle for $LiNbO_3$. These curves are plotted from theoretical data similar to that represented in Fig. 3. The designation of the angles (θ and α) are indicated on the plot.

II. STIMULATED RAMAN SCATTERING FOR AN INFRARED ACTIVE TRANSITION

(R. H. Pantell, H. E. Puthoff and J. A. Gelbwachs)

A. INTRODUCTION

The purposes of this investigation were to study the conversion of energy from one optical frequency to another using the Raman effect; to attempt to develop a continuously-tunable optical source based on the Raman effect; to generate new frequencies in the far infrared; and to obtain a better understanding of the mechanisms involved in this non-linear process.

The principal investigator was Professor Richard H. Pantell, and this contract has supported research in which one research associate and two graduate students participated.

B. MAJOR ACCOMPLISHMENTS AND PROBLEMS ENCOUNTERED

1. Background

Preceding the work undertaken in this study, a detailed analysis of the stimulated Raman effect as applied to tunable lasers was completed. In the stimulated Raman effect as considered here, an optical laser beam passing through a crystal excites a low frequency (infrared) vibrational mode. During the process an optical beam is generated at the Raman frequency (incident minus vibrational mode frequency). The output frequency is tuned as the angle between the laser and Raman beams is changed. The configuration for such a system is shown in Fig. 1. The tunability of the output is due to wavevector conservation, as shown in Figs. 2 and 3. The preparatory

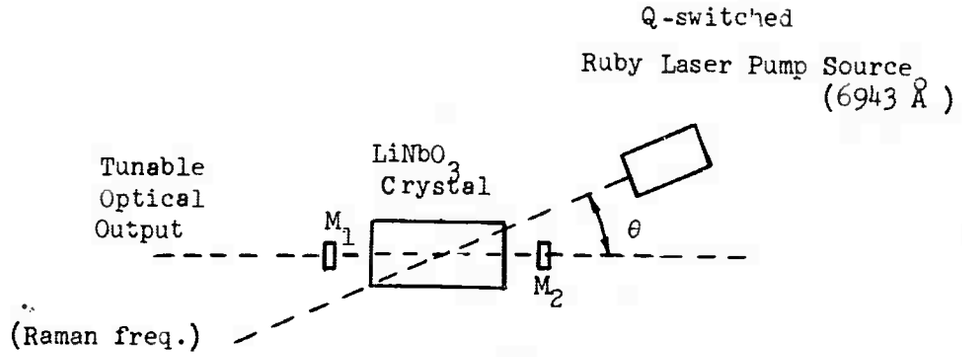

FIG 1--Tunable Raman laser design. The off-axis resonator system allows the angle θ between laser and Stokes beams to be controlled, which in turn determines the frequency of the tunable optical output. Mirror M_1 and M_2 provide for multiple passes of the Raman beam. If the small-signal gain per round trip pass exceeds the loss, then appreciable optical fields can build up within the resonator and thus provide significant Raman output.

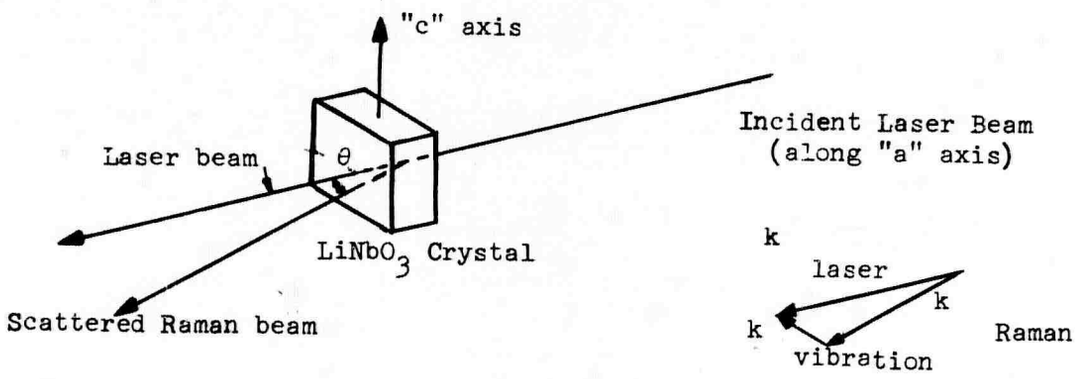

FIG. 2--Experimental geometry indicating how wavevector conservation determines $k_{vibration}$. This, in turn, determines the vibrational frequency and Raman shift as shown in Fig. 3.

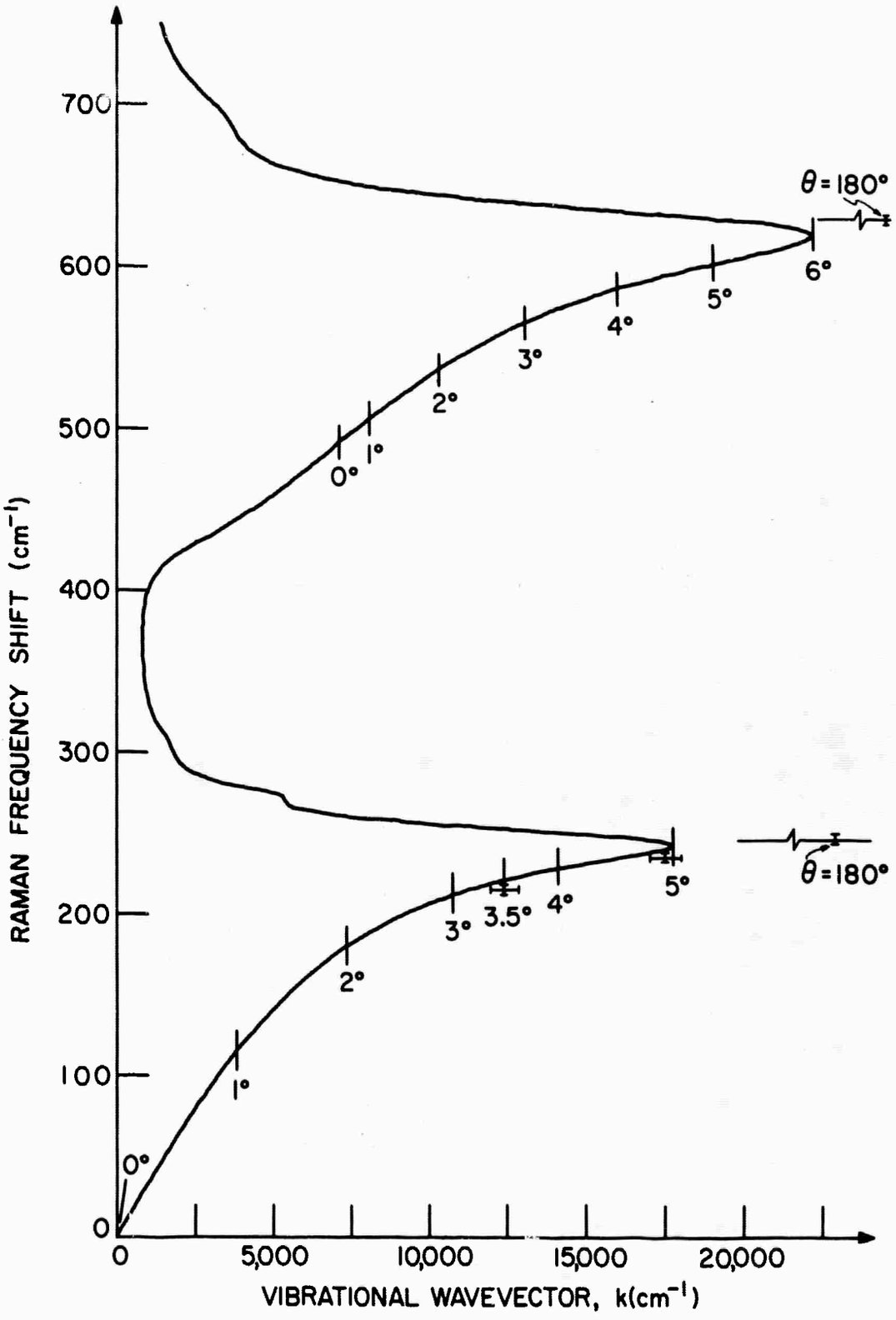

FIG. 3--Raman frequency shift as a function of vibrational wave vector k, where k is determined by wavevector conservation as shown in Fig. 2. The angle θ corresponds to the angle between the Stokes and laser beams determined by the mechanical arrangement of Fig. 1.

study on which the present project was based indicated that the laser pump power required to reach threshold in the crystal $LiNbO_3$ is ~ 4 Mw/cm^2 for a 0.5 cm crystal for both the 248 cm^{-1} and 628 cm^{-1} modes. Such a level is a modest requirement indicating the feasibility of a tunable laser based on the stimulated Raman effect. Concurrent with the generation of a tunable output at the infrared vibrational mode frequency (~ 15 - 20 microns for the mode considered here.)

2. Experimental Work and Results

Under this contract, experimental apparatus was constructed to observe tunable stimulated Raman emission. Over the course of the contract several lithium niobate crystals were grown by the crystal-growing laboratory of the Center for Materials Research, located on campus. The crystals ranged from 1 - 5 cm in length (along the "a" axis) and were anti-reflection coated for the Raman frequency (~ 7260 Å).

Initial experiments with the setup of Fig. 1 yielded inconclusive results in which stimulated Raman emission was apparently obtained on a sporadic non-reproducible basis. Crystal damage occurred in the process.

Concurrent with the experimental work discussed above, theoretical work by Harris[1] at Stanford showed that in parametric processes of this type, only that portion of the pump laser beam which is in a TEM_{oo} gaussian mode is effective in the pumping process. Power in higher order modes is wasted as far as pumping is concerned but can damage the crystal and should therefore be eliminated. As a result, an experimental program for forcing the output into the TEM_{oo} mode

was carried out. The configuration finally chosen is that shown in Fig. 4. As a result of uneven pumping of the ruby rod, the rod acts as a lens which in effect transforms the flat rear mirror into a spherical mirror of radius of curvature ~ 5 - 6 m. The cavity therefore acts as a plano-concave resonator with one flat mirror and one curved mirror. With the aid of the diaphragm to confine the beam, the resultant beam is a TEM_{oo} mode with a power ~ 600 kW in a 0.3 mm^2 area with a beam divergence ~ 3 - 5 milliradians.

In order to improve the alignment procedure for the Raman cavity, one cavity mirror (see Fig. 1) was mounted on a scanning Fabry-Perot mount which permits active tuning of the cavity to a minimum loss configuration, a technique known from other experiments to yield a considerable improvement of the alignment while providing an exact measurement of the cavity losses.

C. FINAL RESULTS

In final experiments carried out just prior to termination of the contract, the system worked extremely well and the entire program turned out to be successful. We were able to report the first observation of tunable stimulated Raman emission. Stimulated Raman scattering from the 152 cm^{-1}, 248 cm^{-1}, and 628 cm^{-1} modes, all of which are tunable was observed. Tuning over several hundred angstroms in the visible and over tens of microns in the infrared are now possible by the technique developed under this contract.

Several interesting features of the tunable Raman oscillator which compare favorably with other forms of parametric oscillators, are that

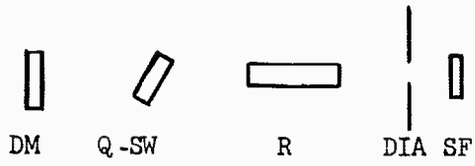

FIG. 4 --Configuration for obtaining low divergence (~ 1 mrad) laser beam. Components: DM, dielectric mirror > 99%; Q-SW, Brewster angle cell containing cryptocyanine dye in methanol for Q-switching; R, 3" x ½" rubyrod; DIA, 2 mm diameter diaphragm; SF, sapphire flat output mirror.

birefringent wavevector matching is not necessary. Operation occurs at any convenient temperature, including room temperature; several discrete frequencies may be generated and tuned simultaneously, including tunable radiation over a broad range in the far infrared, and the generation of anti-Stokes radiation which has been observed provides sources at wavelengths shorter than the wavelength of the pump.

A summary of the experimental results for the tunable stimulated Raman oscillator is given in Appendix A.

APPENDIX A

A TUNABLE STIMULATED RAMAN OSCILLATOR

by

J. Gelwachs, R. H. Pantell, H. E. Puthoff, J. M. Yarborough

A TUNABLE STIMULATED RAMAN OSCILLATOR*

by

J. Gelbwachs, R. H. Pantell, H. E. Puthoff, J. M. Yarborought†

Stanford University

Stanford, California

We report the first observation of tunable stimulated Raman emission. A Q-switched ruby laser was used to excite the A_1 symmetry 248 cm^{-1} polariton mode in a $LiNbO_3$ crystal. The crystal, at room temperature, was placed in a resonator external to the laser cavity which was tuned to the Stokes frequency. It was possible to vary the Stokes frequency by altering the angle between the pump beam and the axis of the resonator. Stimulated Raman scattering from other polariton modes (152 cm^{-1}, 628 cm^{-1}) which are potentially tunable was observed. We also report the first observation of stimulated anti-Stokes emission from a polariton mode.

* This work was supported in part by the U. S. Army Research Office, the U. S. Air Force Office of Scientific Research, and the U. S. Office of Naval Research under the Joint Services Electronics Program by Contract Nonr 225(48) and in part by the U. S. Office of Naval Research under Contract NOCO14-67-A-0112-0018.

† J. M. Yarborough is being partially supported by the Sylvania independent research program.

A transverse optical lattice mode which is infrared absorbing has a mode frequency that is dependent on wavevector, as shown in Fig. 1. The mode energy is partially mechanical and partially electromagnetic, and the corresponding quanta of the mixed mode have been termed polaritons.[1-3] Dispersion curves have been determined experimentally for $LiNbO_3$[4] and other crystals[5-7] by the observation of near-forward spontaneous Raman scattering at the Stokes frequency. The possibility of constructing a tunable stimulated Raman oscillator based on this effect was considered in detail in a previous paper.[8]

In this letter we report the observation of stimulated Raman scattering (SRS) from several polariton modes in $LiNbO_3$, including tunable emission from one of these modes. There have been previous reports of SRS from infrared active vibrations generated in a direction that is collinear with the pump beam.[9-13] To obtain tunable emission we provided an off axis resonator external to the laser source so that the generation of Stokes light took place at an angle θ relative to the direction of propagation of the incident pump source.[8,14] As θ was varied, the Stokes frequency changed.

The tuning characteristic of a $LiNbO_3$ Raman oscillator is determined by wavevector conservation and the dispersion curve,[4] as illustrated in Fig. 1. The polariton frequency which determines the Stokes shift is shown as a function of wavevector, and the short intersecting lines are obtained from wavevector conservation as a function of the angle θ inside the crystal.

Figure 2 is an illustration of the apparatus used in this experiment. The pump source was a ruby laser, which was Q-switched by a

cryptocyanine dye. A 2 mm aperture was placed inside the laser cavity to inhibit the excitation of high order transverse modes. The laser emitted pulses of 20 nsec duration with a peak power of approximately 2 Mw, and a 2 mm beam diameter. An external resonator was provided for the $LiNbO_3$ crystal which consisted of two mirrors placed 8 cm apart. One mirror was flat and the other was spherical with a 130 cm radius, and each mirror had a reflectivity of about 99.5% at the Stokes wavelength. The laser beam made a single pass through this interferometer. A piezoelectric transducer was used as a mount for one mirror to provide scanning to facilitate resonator alignment. The crystal was anti-reflection coated, but at the power densities used in the experiment the coatings were damaged after several laser pulses. The time response of the Stokes emission was recorded by placing a photo-multiplier at the exit slit of a prism spectrometer, and the wavelengths were recorded on film placed at the output of a 2 m grating spectrometer.

Figure 3a was obtained from the grating spectrometer with the resonator for the Stokes light aligned at an angle $\theta = 3.5^\circ$ inside the crystal relative to the propagation direction for the pump beam. Polarization of the ruby laser was along the c axis. A 60 cm focal length lens was used to focus a 1.5 Mw beam to a diameter of approximately 1.2 mm in a $LiNbO_3$ crystal 1.5 cm long. Some scattered ruby light at 6943 Å appears as the line on the left, and the SRS is shown as the line on the right shifted 214 cm^{-1} from the ruby. This data point has been marked on the dispersion curve in Fig. 1. Figure 3b shows the ruby and Stokes lines for an angle $\theta = 5^\circ$, where the frequency difference is now 235 cm^{-1}. This point is also recorded on Fig.1.

Back scattered Stokes emission was obtained for both the 248 cm^{-1} and 628 cm^{-1} modes as shown in Fig. 3c. In this case the external resonator was not used and a 44 cm focal length lens focused a 2.7 Mw beam to a diameter of approximately 0.9 mm in a 3.2 cm $LiNbO_3$ crystal. Emission in the back direction was reflected from a glass slide into the spectrometer. The Stokes shifts for the back scattered ($\theta = 180^{\circ}$) lines in Fig. 3c are 250 cm^{-1} and 628 cm^{-1}, and these two points have been marked on Fig. 1.

We also observed emission from what we interpret to be the 152 cm^{-1} E symmetry mode when we used the 3.2 cm crystal inside the external resonator at an angle $\theta = 5^{\circ}$. This emission line is shown in Fig 3e. The 248 cm^{-1} mode was not observed in this crystal for off-axis pumping. It is possible to tune the 152 cm^{-1} mode in the same manner as the A_1 symmetry modes. Presumably variations in material properties from one crystal sample to another could be responsible for the generation of one mode of vibration in preference to another. Although it is not visible in Fig. 3e, there is also a weak line corresponding to the 628 cm^{-1} mode. It is interesting to note that for this crystal the 152 cm^{-1} mode was the most intense when placed in a resonator at $\theta = 5^{\circ}$, whereas for the back-scattered direction emission was obtained only for the 248 cm^{-1} and 628 cm^{-1} modes.

After several laser pulses which yielded no SRS, we opened the input slit of the spectrometer to increase the acceptance angle. On one shot for which the slit was opened wide we obtained the photograph in Fig. 3f. This was for the 1.5 cm crystal pumped at an angle $\theta = 3.5^{\circ}$. By means of a neon lamp light source we determined that the wide-slit

ines collapse to the positions shown by the arrows as the slit is narrowed. Line 1 is the ruby. Line 2 corresponds to Stokes scattering of the ruby light from the 248 cm^{-1} mode at an angle $\theta = 3.5^{\circ}$. Line 5 is the 180° scattering from the 628 cm^{-1} mode with line 2 as the pump source. The Stokes radiation from the 248 cm^{-1} mode is more effective as a pump source than the laser because the ruby light makes a single pass through the resonator; also, there is a longer interaction length for the Stokes beam because it is collinear with the cavity axis.

Lines 3, 4 and 6 are open to several interpretations, but we believe the most probable explanations are as follows. Line 3 results from 180° scattering from the 248 cm^{-1} mode and line 4 is 0° scattering from the 628 cm^{-1} mode, both with line 2 as the pump source. Line 6 is caused by 0° scattering from the 628 cm^{-1} mode with line 3 as the pump source.

We obtained Fig. 4 by focusing the ruby beam with a 13 cm focal length lens into a 1.4 cm crystal and imaging light scattered in the forward direction, which includes reflected back-scattered light, onto the spectrometer slit. No external resonator was used, and the central portion of the ruby beam out of the crystal was blocked with a 2 mm mask. In Fig. 4 wavelength increases to the right, and we interpret the photograph as follows. Line 3 is the ruby laser pump source; line 7, shifted 628 cm^{-1} from the ruby line, corresponds to back scattering from the 628 cm^{-1} mode; line 6, shifted 492 cm^{-1} from the ruby line, corresponds to $\sim 0^{\circ}$ scattering from the 628 cm^{-1} mode; line 1 is the anti-Stokes line associated with line 6. Line 5 corresponds to back scattered Stokes radiation from the 248 cm^{-1} mode. Line 4, shifted

152 cm^{-1} from the ruby line to a longer wavelength, is back-scattering from the ruby to a shorter wavelength. It is not obvious what mechanism produces line 2. A possible explanation is that this line results from mixing between line 4 and reflected laser light.

The resonator losses at the Stokes wavelengths are about 5% per round trip which, for the 248 cm^{-1} mode, requires a laser power density of approximately 4 Mw/cm^2 for gain to exceed losses.[15] Our peak power density generally exceeded 100 Mw/cm^2 so that we were well above the threshold level, and it is probable that laser depletion occurred towards the end of the Q-switched pulse.

In addition to generating emission at the Stokes frequencies we can assume that stimulated emission at the various polariton frequencies was also produced. The shortest vibrational wavelength we stimulated was 16 μ and the longest was 66 μ. In scattering from the 248 cm^{-1} mode the loss in the crystal is quite small for wavelengths greater than 50 μ and therefore reasonable power levels might be expected in this region.

We succeeded in tuning the frequency of the Stokes radiation from the 248 cm^{-1} mode by 36 cm^{-1}, but by using both the 628 cm^{-1} and the 248 cm^{-1} modes it should be possible to obtain tuning over $\sim$ 350 cm^{-1}.

Some interesting features of the tunable Raman oscillator are that birefringent wavevector matching is not necessary; operation occurs at any convenient temperature; several discrete frequencies may be generated and tuned simultaneously, including tunable radiation over a broad range in the far infrared; and the generation of anti-Stokes

radiation provides sources at wavelengths shorter than the wavelength of the pump.

The authors gratefully acknowledge the efforts of R. Feigelson of the Stanford Center for Materials Research who grew the crystals used in this experiment. The dispersion curve shown in Fig 1 was provided by Mr. S. Sussman. We appreciate the technical assistance of D. Hecht and M. Chacon and acknowledge helpful discussions with B. G. Huth and G. Soncini during the early stages of this work.

REFERENCES

1. K. Huang, Proc. Roy. Soc. (London) A208, 352 (1951).
2. M. Born and K. Huang, Dynamical Theory of Crystal Lattices, Clarendon Press, Oxford, England (1954), pp. 82 ff.
3. A. S. Barker, Jr., Phys. Rev. 136, A1290 (1964).
4. H. E. Puthoff, R. H. Pantell, B. G. Huth, and M. A. Chacon, J. Appl. Phys. 39, 2144 (1968).
5. C. H. Henry and J. J. Hopfield, Phys. Rev. Lett. 15, 964 (1965).
6. S. P. S. Porto, B. Tell, and T. C. Damen, Phys. Rev. Letters 16, 450 (1966).
7. J. F. Scott and S. P. S. Porto, Phys Rev. 161, 903 (1967).
8. H. E. Puthoff, R. H. Pantell, and B. G. Huth, J. Appl. Phys. 37, 860 (1966). (In this paper the results of the analysis were applied to an anisotropic molecule in an isotropic configuration. Symmetry considerations preclude tuning in this case, and therefore the example was inappropriate.)
9. P. E. Tannenwald and J. B. Thaxter, Science 154, 1319 (1966).
10. M. D. Martin and E. L. Thomas, IEEE J. Quant. Electron. QE-2, 196 (1966).
11. P. E. Tannenwald and D. L. Weinberg, IEEE J. Quant. Electron. QE-3, 334 (1967).
12. P. E. Tannenwald, J. Appl. Phys. 38, 4788 (1967).
13. S. K. Kurtz and J. A. Giordmaine, to be published.

14. H. E. Puthoff, Microwave Lab Report 1547, Stanford University, Stanford, California.

15. W. D. Johnston, Jr., I. P. Kaminow, and J. G. Bergman, Jr., Appl. Phys. Letters 13, 190 (1968).

FIGURE CAPTIONS

1. Dispersion characteristic for A symmetry modes in $LiNbO_3$.
2. Schematic diagram of the experimental apparatus. Lens L_1 focuses the Q-switched ruby beam into the $LiNbO_3$ crystal. Mirrors M_1 and M_2 are highly reflecting at the Stokes wavelengths. PZT is a piezoelectric transducer to sweep mirror M_2 so that the resonator may be used as a scanning Fabry-Perot for alignment purposes. MC_1 is a monochrometer set to the Stokes wavelength with a photomultiplier PMT placed at the exit slit. Lens L_2 images the Stokes beam onto the entrance slit of monochrometer MC_2, and the output from this monochrometer is recorded on film.
3. Stimulated Stokes spectra (a) $\theta = 3.5^\circ$, 1.5 cm crystal; (b) $\theta = 5^\circ$, 1.5 cm crystal; (c) $\theta = 180^\circ$, 3.2 cm crystal; (d) neon calibration spectrum; (e) $\theta = 5^\circ$, 3.2 cm crystal; (f) $\theta = 3.5^\circ$, 1.5 cm crystal.
4. Stimulated Stokes and anti-Stokes spectra from a 1.4 cm crystal.

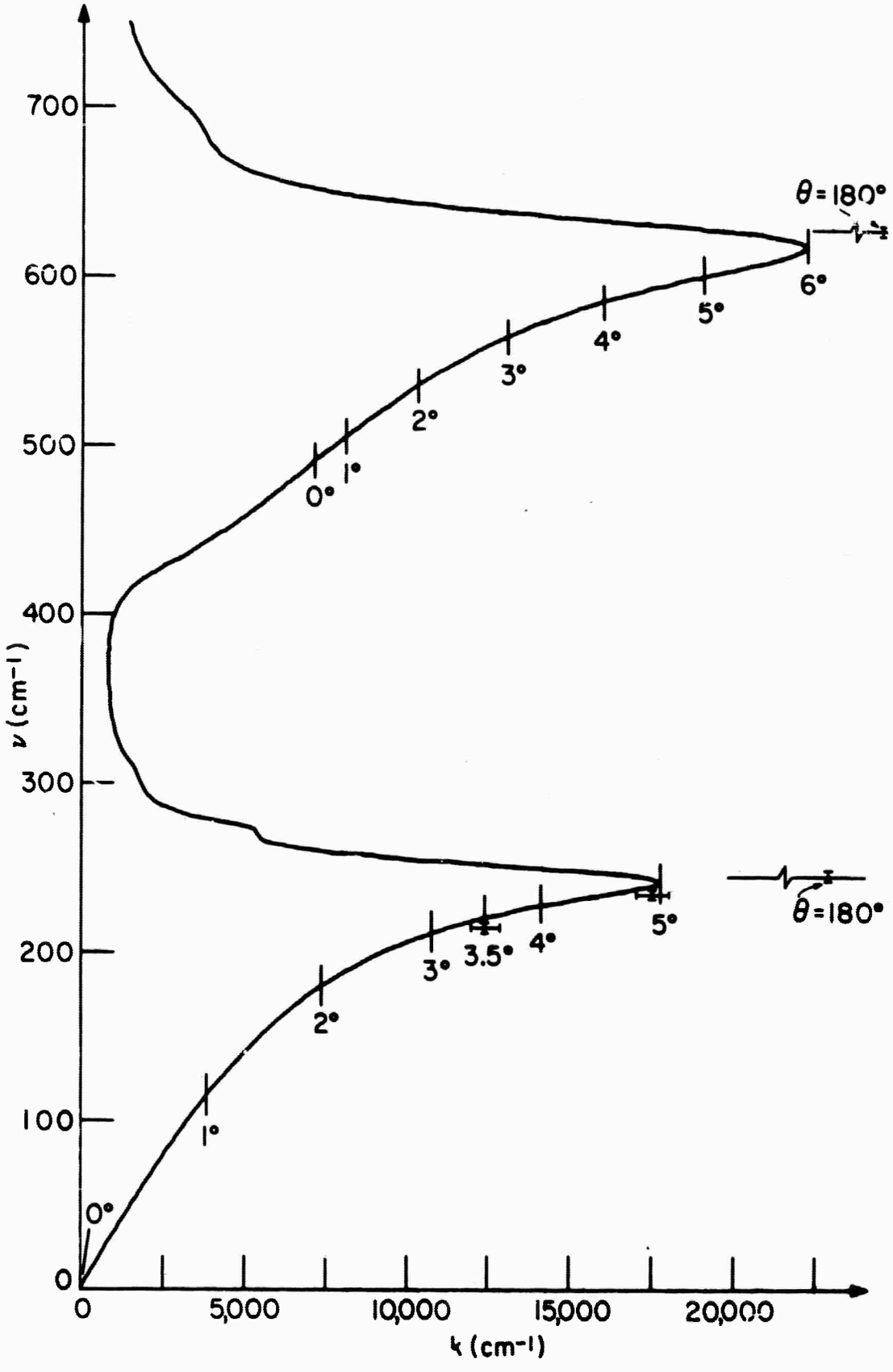
700
600
500
400
300
200
100
0
ν (cm⁻¹)
θ = 180°
6°
5°
4°
3°
2°
1°
0°
θ = 180°
5°
4°
3.5°
3°
2°
1°
0°
0
5,000
10,000
15,000
20,000
k (cm⁻¹)

FIGURE 1

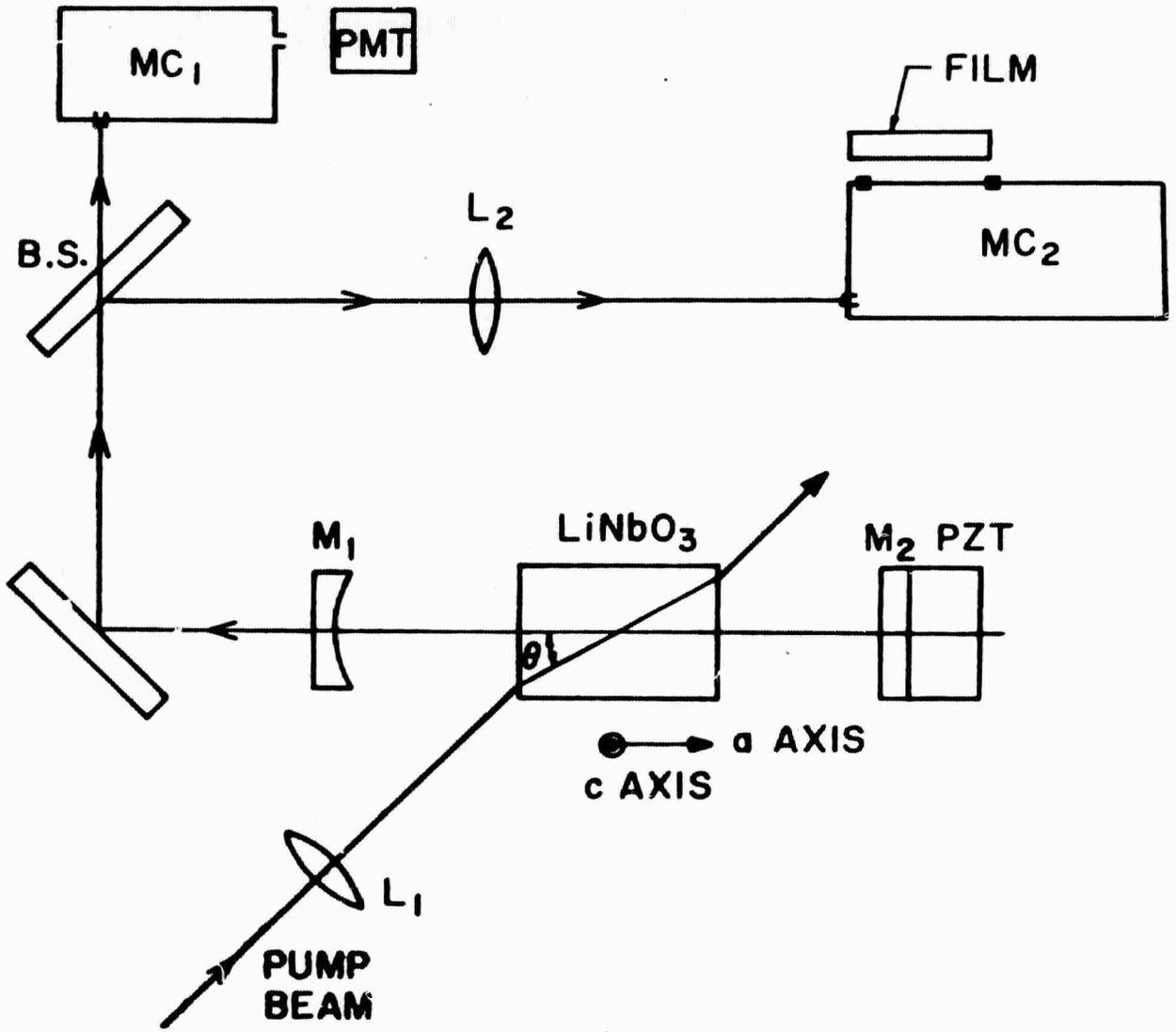
MC1
PMT
FILM
L2
B.S.
MC2
M1
LiNbO3
M2 PZT
θi
a AXIS
c AXIS
L1
PUMP
BEAM

FIGURE 2

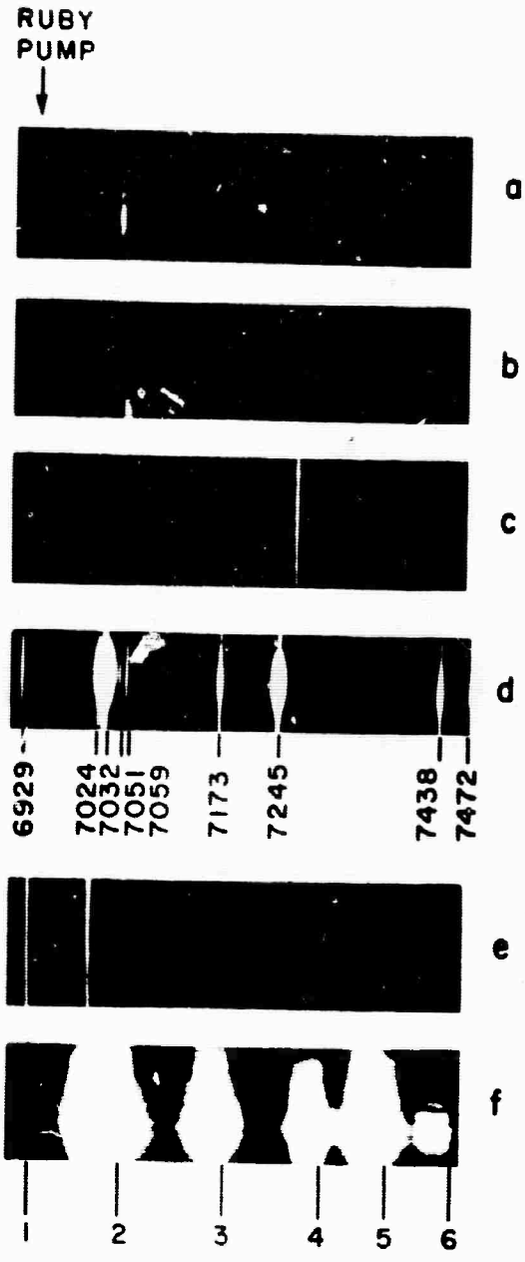
RUBY
PUMP
a
b
c
d
6929
7024
7032
7051
7059
7173
7245
7438
7472
e
f
1
2
3
4
5
6

FIGURE 3

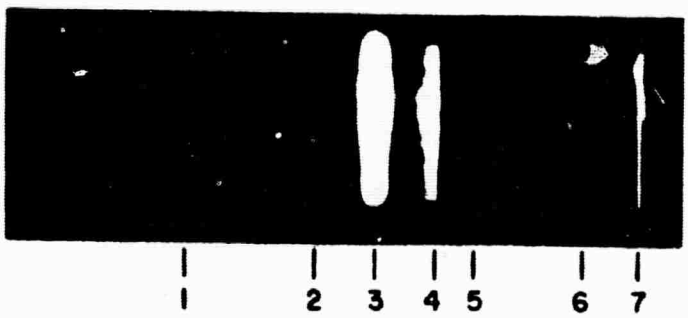

FIGURE 4